Vectorial structure and beam quality of vector-vortex Bessel–Gauss beams in the far field

Lina Guo (郭利娜)[1,2] and Zhilie Tang (唐志列)[1*]

[1]*School of Physics and Telecommunication Engineering, Laboratory of Quantum Information Technology, South China Normal University, Guangzhou 510006, China*

[2]*School of Electronics and Information, GuangDong Polytechnic Normal University, Guangzhou 510665, China*

[*]*Corresponding author: tangzhil@scnu.edu.cn*

Received August 25, 2011; accepted October 24, 2011; posted online May 9, 2012

The far-field analytical expressions for the electromagnetic fields of amplitude of vector-vortex beams having a Bessel–Gauss (BG) distribution propagating in free space are obtained based on the vector angular spectrum and the method of stationary phase. The far-field energy flux distributions and the beam quality by the power in the bucket (PIB) in the paraxial and nonparaxial regimes are investigated. The PIB of the vector-vortex BG beams depend on the ratio of the waist width to wavelength and the polarization order. The analyses show that vector-vortex BG beams with low polarization order have better energy focusability in the far field.

OCIS codes: 260.2110, 350.5500, 260.5430.

doi: 10.3788/COL201210.S12601.

In recent years, cylindrically vector beams, such as radially polarized beams, have received lots of attention because of their interesting properties and practical applications[1]. Various methods to achieve such an inhomogeneous polarization state of a laser beam have been exploited by many researchers[2]. Many propagation researches are conducted within and beyond the paraxial regime. The nonparaxial derivation of radially polarized beams is performed and analyzed by the method of Rayleigh-Sommerfeld diffraction integrals[3,4]. The paraxial propagation of radially polarized beams has been dealt with as special cases of nonparaxial results[4]. Also paraxial propagation of radially polarized beams is analyzed by a q-parameter approach in Ref. [5]. The analytical vectorial structures of radially polarized beams in free space have been investigated in Ref. [6]. The far field energy flux distribution and the beam quality of cylindrically polarized vector beam in the nonparaxial regime have been presented in Ref. [7]. Recently, vector-vortex beams that have more than one rotation of the polarization have attracted increased interest[8,9]. Due to their strange axial electric and magnetic field distributions, vector-vortex beams may find interesting applications in many areas like spectroscopy, high resolution microscopy, optical tweezers, and quantum communication[10].

In this letter, by means of the full vector angular spectrum of electromagnetic wave and the method of stationary phase, the analytical expressions of the TE and TM terms of vector-vortex beams having a Bessel–Gauss (BG) distribution are presented in the far field. The corresponding energy flux distributions of the TE term, the TM term, and power in the bucket (PIB) are also investigated in the far field.

The electric field distribution of a BG vector-vortex beam at the $z = 0$ plane reads as

$$E_x(x,y,0) = E_0 J_{\mathrm{n}}(\alpha r)\exp\left(-\frac{r^2}{w_0^2}\right)\cos(n\varphi), \tag{1a}$$

$$E_y(x,y,0) = E_0 J_{\mathrm{n}}(\alpha r)\exp\left(-\frac{r^2}{w_0^2}\right)\sin(n\varphi), \tag{1b}$$

where E_0 is a constant, n is the polarization order of vector-vortex beam which determines the spatial polarization pattern[9], $J_n(\cdot)$ is the nth order of Bessel function of the first kind, w_0 is the beam waist width, $r = \left(x^2 + y^2\right)^{1/2}$ and $\varphi = \arctan(y/x)$ are the radial and azimuthal coordinates, respectively. Obviously, radially polarized beam ($n = 1$) is $n = 1$ vector-vortex beams.

According to the vectorial structure of non-paraxial electromagnetic beam[11,12], an arbitrary polarized electromagnetic field can be expressed as the sum of two terms $\vec{E}_{\mathrm{TE}}(\vec{r})$ and $\vec{E}_{\mathrm{TM}}(\vec{r})$, namely,

$$\begin{aligned}
\vec{E}(\vec{r}) =& \vec{E}_{\mathrm{TE}}(\vec{r}) + \vec{E}_{\mathrm{TM}}(\vec{r}),\\
\vec{E}_{\mathrm{TE}}(\vec{r}) =& \int\int_{-\infty}^{\infty}\frac{1}{b^2}\left[qA_x(p,q) - pA_y(p,q)\right]\\
&(q\vec{e}_x - p\vec{e}_y)\exp(\mathrm{i}km)\,\mathrm{d}p\mathrm{d}q,\\
\vec{E}_{\mathrm{TM}}(\vec{r}) =& \int\int_{-\infty}^{\infty}\frac{1}{b^2}\left[pA_x(p,q) + qA_y(p,q)\right]\\
&\left(p\vec{e}_x + q\vec{e}_y - \frac{b^2}{\gamma}\vec{e}_z\right)\exp(\mathrm{i}km)\mathrm{d}p\mathrm{d}q,
\end{aligned} \tag{2}$$

where $\vec{r} = x\vec{e}_x + y\vec{e}_y + z\vec{e}_z$ is the location vector; $m = px + qy + \gamma z$; $b^2 = p^2 + q^2$; $\gamma = \left(1 - p^2 - q^2\right)^{1/2}$; $k = 2\pi/\lambda$ with λ being the optical wavelength. $A_x(p,q,\gamma)$ and $A_y(p,q,\gamma)$ are the x and y components of the vector angular spectrum, respectively, and are obtained by Fourier transforming the x and y components of the initial electric field,

$$\begin{aligned}
\vec{A}(p,q,\gamma) =& \begin{pmatrix} A_x(p,q,\gamma) \\ A_y(p,q,\gamma) \end{pmatrix}\\
=& \frac{1}{\lambda^2}\int_{-\infty}^{\infty}\int_{-\infty}^{\infty}E(x,y,0)\exp\left[-\mathrm{i}k(px+qy)\right]\mathrm{d}x\mathrm{d}y
\end{aligned}$$

$$
\begin{aligned}
=&\frac{\pi E_0 w_0^2 \mathrm{i}^n}{\lambda^2}\begin{pmatrix}\cos(n\psi)\\ \sin(n\psi)\end{pmatrix}\\
&\cdot\exp\left[-\frac{\alpha^2 w_0^2+k^2 w_0^2\left(p^2+q^2\right)}{4}\right]\\
&\times I_n\left(\frac{k\alpha w_0^2\sqrt{p^2+q^2}}{2}\right).
\end{aligned}\tag{3}
$$

Similarly, the magnetic field can also be expressed as a sum of two terms, $\overrightarrow{H}_{\mathrm{TE}}(\overrightarrow{r})$ and $\overrightarrow{H}_{\mathrm{TM}}(\overrightarrow{r})$[10,11],

$$
\begin{aligned}
\overrightarrow{H}(\overrightarrow{r}) =&\overrightarrow{H}_{\mathrm{TE}}(\overrightarrow{r})+\overrightarrow{H}_{\mathrm{TM}}(\overrightarrow{r}),\\
\overrightarrow{H}_{\mathrm{TE}}(\overrightarrow{r}) =&\sqrt{\frac{\varepsilon}{\mu}}\int\int_{-\infty}^{\infty}\frac{1}{b^2}\left[qA_x(p,q)-pA_y(p,q)\right]\\
&\cdot\left(p\gamma\overrightarrow{e}_x+q\gamma\overrightarrow{e}_y-b^2\overrightarrow{e}_z\right)\times\exp(\mathrm{i}km)\,\mathrm{d}p\mathrm{d}q,\\
\overrightarrow{H}_{\mathrm{TM}}(\overrightarrow{r}) =&-\sqrt{\frac{\varepsilon}{\mu}}\int\int_{-\infty}^{\infty}\frac{1}{b^2\gamma}\left[pA_x(p,q)+qA_y(p,q)\right]\\
&\cdot\left(q\overrightarrow{e}_x-p\overrightarrow{e}_y\right)\times\exp(\mathrm{i}km)\,\mathrm{d}p\mathrm{d}q,
\end{aligned}\tag{4}
$$

where ε and μ are the electric permittivity and magnetic permeability in medium, respectively. Since z is big enough in the far regime, the condition of $kr\to\infty$ and $r=\left(x^2+y^2+z^2\right)^{1/2}$ are satisfied and the contribution of the evanescent waves to the far field can be omitted. By employing the method of stationary phase[13−15], the analytical electromagnetic fields of the TE mode for BG vector-vortex beams in the far field may be given by

$$
\begin{aligned}
\overrightarrow{E}_{\mathrm{TE}}(\overrightarrow{r}) =&\frac{Z_{\mathrm{R}}E_0 z\mathrm{i}^{n+1}}{\rho r^2}\sin\left[(n-1)\theta\right]\\
&\cdot\exp\left(\mathrm{i}kr-\frac{\alpha^2 w_0^2 r^2+k^2 w_0^2\rho^2}{4r^2}\right)\\
&\times I_n\left(\frac{k\alpha w_0^2\rho}{2r}\right)\left(y\overrightarrow{e}_x-x\overrightarrow{e}_y\right),
\end{aligned}\tag{5}
$$

$$
\begin{aligned}
\overrightarrow{H}_{\mathrm{TE}}(\overrightarrow{r}) =&\sqrt{\frac{\varepsilon}{\mu}}\frac{Z_{\mathrm{R}}E_0 z\mathrm{i}^{n+1}}{\rho r^3}\sin\left[(n-1)\theta\right]\\
&\cdot\exp\left(\mathrm{i}kr-\frac{\alpha^2 w_0^2 r^2+k^2 w_0^2\rho^2}{4r^2}\right)\\
&\times I_n\left(\frac{k\alpha w_0^2\rho}{2r}\right)\left(xz\overrightarrow{e}_x+yz\overrightarrow{e}_y-\rho^2\overrightarrow{e}_z\right),
\end{aligned}\tag{6}
$$

with $Z_{\mathrm{R}}=kw_0^2/2$ is Rayleigh distance, $\rho=\left(x^2+y^2\right)^{1/2}$ and $I_n(\cdot)$ is the modified Bessel function of the first kind. Similarly, the analytical electromagnetic fields of the TM mode for BG vector-vortex beams in the far field may be given by

$$
\begin{aligned}
\overrightarrow{E}_{\mathrm{TM}}(\overrightarrow{r}) =&-\frac{Z_{\mathrm{R}}E_0\mathrm{i}^{n+1}}{\rho r^2}\cos\left[(n-1)\theta\right]\\
&\cdot\exp\left(\mathrm{i}kr-\frac{\alpha^2 w_0^2 r^2+k^2 w_0^2\rho^2}{4r^2}\right)\\
&\times I_n\left(\frac{k\alpha w_0^2\rho}{2r}\right)\left(xz\overrightarrow{e}_x+yz\overrightarrow{e}_y-\rho^2\overrightarrow{e}_z\right),
\end{aligned}\tag{7}
$$

$$
\begin{aligned}
\overrightarrow{H}_{\mathrm{TM}}(\overrightarrow{r}) =&\sqrt{\frac{\varepsilon}{\mu}}\frac{Z_R E_0\mathrm{i}^{n+1}}{r\rho}\cos\left[(n-1)\theta\right]\\
&\cdot\exp\left(\mathrm{i}kr-\frac{\alpha^2 w_0^2 r^2+k^2 w_0^2\rho^2}{4r^2}\right)\\
&\times I_n\left(\frac{k\alpha w_0^2\rho}{2r}\right)\left(y\overrightarrow{e}_x-x\overrightarrow{e}_y\right).
\end{aligned}\tag{8}
$$

Equations (5)–(8) constitute the basic results obtained in this letter; they are applicable for both paraxial case and non-paraxial case. As indicated by Eqs. (5)–(8), the TE and TM terms of vectorial BG vector-vortex beams are orthogonal to each other.

The energy flux distribution at the $z=$ const plane are given by the z component of their time average Poynting vector. From Eqs. (5)–(6), the energy flux distribution of the TE term for BG vector-vortex beams at the far field $z=$ const plane is given by

$$
\begin{aligned}
\langle S_z\rangle_{\mathrm{TE}} =&\frac{1}{2}\mathrm{Re}\left(E_{\mathrm{TE}}^*\times H_{\mathrm{TE}}\right)_z\\
=&\sqrt{\frac{\varepsilon}{\mu}}\frac{Z_{\mathrm{R}}^2E_0^2z^3}{2\rho^2r^3}\sin^2\left[(n-1)\theta\right]\\
&\cdot\exp\left(-\frac{\alpha^2 w_0^2 r^2+k^2 w_0^2\rho^2}{2r^2}\right)\times I_n^2\left(\frac{k\alpha w_0^2\rho}{2r}\right),
\end{aligned}\tag{9}
$$

where Re represents the real part, and the asterisk denotes complex conjugation. From Eqs. (7) and (8), the energy flux distribution of the TM term for BG vector-vortex beams at the far field $z=$ const plane is given by

$$
\begin{aligned}
\langle S_z\rangle_{\mathrm{TM}} =&\frac{1}{2}\mathrm{Re}\left(E_{\mathrm{TM}}^*\times H_{\mathrm{TM}}\right)_z\\
=&\sqrt{\frac{\varepsilon}{\mu}}\frac{Z_{\mathrm{R}}^2E_0^2z}{2r\rho^2}\cos^2\left[(n-1)\theta\right]\\
&\cdot\exp\left(-\frac{\alpha^2 w_0^2 r^2+k^2 w_0^2\rho^2}{2r^2}\right)\times I_n^2\left(\frac{k\alpha w_0^2\rho}{2r}\right).
\end{aligned}\tag{10}
$$

Equations (9) and (10) indicate that, radially polarized beam ($n=1$) has no TE component, which is agree with the result of Ref. [6]. From Eqs. (9) and (10), the energy flux distribution at the far field $z=$ const plane turns out to be

$$
\begin{aligned}
\langle S_z\rangle =&\langle S_z\rangle_{\mathrm{TE}}+\langle S_z\rangle_{\mathrm{TM}}\\
=&\sqrt{\frac{\varepsilon}{\mu}}\frac{Z_{\mathrm{R}}^2E_0^2z^3}{2\rho^2r^3}\exp\left(-\frac{\alpha^2 w_0^2 r^2+k^2 w_0^2\rho^2}{2r^2}\right)I_n^2\\
&\cdot\left(\frac{k\alpha w_0^2\rho}{2r}\right)\times\left\{1+\frac{\rho^2}{z^2}\cos^2\left[(n-1)\theta\right]\right\}.
\end{aligned}\tag{11}
$$

As an alternative approach for characterizing the beam quality in the far field, the PIB in the nonparaxial regime is presented[16]

$$
\mathrm{PIB}=\frac{\int_0^{2\pi}\int_0^a\langle S_z\rangle r\mathrm{d}r\mathrm{d}\theta}{\int_0^{2\pi}\int_0^\infty\langle S_z\rangle r\mathrm{d}r\mathrm{d}\theta},\tag{12}
$$

where a is the bucket radius. The larger value of PIB means the better beam quality and the better energy focusability in the far field.

The energy flux distributions of the TE term, the TM term, and the whole of a BG vector-vortex beam as well as PIB in the far field are examined by using the formulae derived above. As the BG vector-vortex beam is determined by the w_0/λ, and polarization order, we investigate the influence of these parameters on the energy flux distributions. In our calculations, ε/μ is set to be unity and the far-field reference plane is z=10z_{R}. The normalized TE term, TM term, and whole beam energy flux distributions of the BG vector-vortex beams at the plane z=10z_{R} for beam order n= 2 are depicted by Fig. 1. The used parameter is $w_0 = 5\lambda$, which corresponds to the paraxial propagation case. The pattern of the energy flux distributions of the TE and TM terms both possess the two-lobe structure, which are similar to a pair of eyes. Moreover, the energy flux distribution of the TE term elongates parallel to the y-axis, and that of the TM term elongates parallel to the x-axis. Since the number of the lobes depends on the order n, one can judge that the different polarization orders result in the different beam lobe pattern.

Figure 2 shows the energy flux distributions of a BG vector-vortex beam at the plane z=10z_{R} in the paraxial beyond region ($w_0 = 0.2\lambda$), the other parameters are the same as Fig. 1. Compared with Fig. 1, it can be seen that the pattern of the lobes in the two figures is similar. Additionally, the magnitude of the energy flux of the TE term is slightly smaller than that of the TM term in the nonparaxial region. Moreover, the size of the pattern of the TE term is also distinctly smaller than that of the TM term. When the TE and TM terms superpose, the energy flux distribution of the BG vector-vortex beam possesses twofold symmetry. The reason for this phenomenon can be explained as: when the BG vector-vortex beam diffracts in the far field for the nonparaxial case, its TE term is a little larger than TM term, so the energy flux intensity turns out two fold

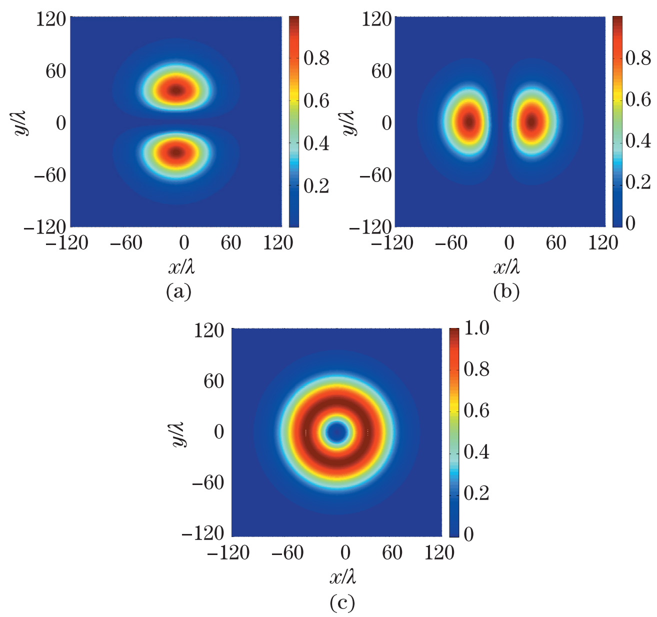

Fig. 1. Energy flux distribution of a BG vector-vortex beam in the plane $z = 10z_{\mathrm{R}}$. $\omega_0 = 5\lambda$, $n = 2$. (a) TE term, (b) TM term, and (c) the whole beam.

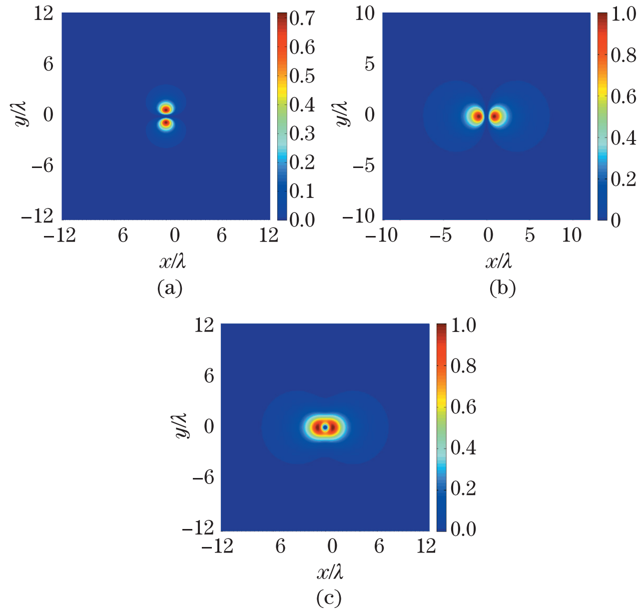

Fig. 2. Energy flux distribution of BG vector-vortex beams in the plane z=10z_R. $\omega_0 = 0.2\lambda$, other parameters are the same as Fig. 2. (a) TE term, (b) TM term, and (c) the whole beam.

axis of symmetry. This result can be observed from the difference in mathematical structures between Eqs. (9) and (10).

Figure 3 exhibits $\langle S_z \rangle$ and PIB curves of vector-vortex BG beams in the far field with different n. One can see that the energy flux distribution of the whole beam for beam order $n = 1$ is no longer doughnutlike and has an intensity peak on the beam axis in the far field, which is different from the result of Ref. [6]. Whereas, the whole energy flux distribution retains a rotationally symmetric dark hollow structure with a single bright ring when $n \geqslant 2$. It can be alse seen that when the beam order n increases, the far-field energy flux distributions would diverge and spread out more rapidly. Figure 3(b) shows that the value of PIB decrease with n increasing. It implies that radial polarization compared with vector vortex polarization has better beam quality and better energy focusability in the far field, which is consistent with the result of Fig. 3(a).

Figure 4(a) exhibits $\langle S_z \rangle$ and PIB curves of vector-vortex BG beams in the far field with different w_0/λ. Note that the energy flux retains dark center, and its profile expands with w_0/λ increasing. From Fig. 4(b), one can find that the value of PIB decreases with w_0/λ increasing. It implies that beam quality and energy focusability of BG vector-vortex beams decrease with w_0/λ increasing.

In conclusions, the energy flux distributions of the TE term, the TM term, and the whole energy flux of BG vector-vortex beams are derived in the far field which are applicable to both nonparaxial case and paraxial case. The results show that the asymmetry of energy flux spot becomes apparent with increasing nonparaxiality. Additionally, energy distributions spread more widely in the far field when beam polarization order n increases. And the value of PIB decreases with n and w_0/λ increasing. This work is also important to understand the

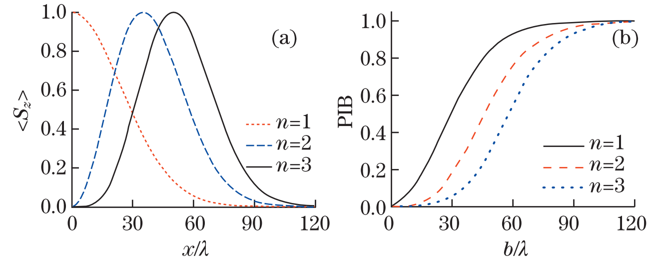

Fig. 3. (a) $\langle S_z \rangle$ and (b) PIB curves of vector-vortex BG beams in the far field with different n. $w_0 = 5\lambda$, the other parameters are the same as those in Fig. 1.

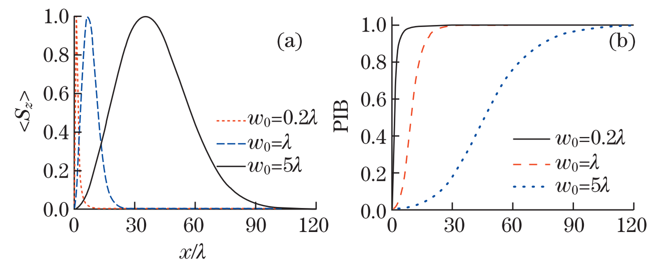

Fig. 4. (a) $\langle S_z \rangle$ and (b) PIB curves of vector-vortex BG beams in the far field with different w_0/λ. $n = 2$, the other parameters are the same as those in Fig. 1.

theoretical aspects of BG vector-vortex beam propagation and is beneficial to its practical application.

This work was supported by the National Natural Science Foundation of China (No. 61178086), the Research Fund for the Doctoral Program of Higher Education of China (No. 20104407110008), and the Youth Foundation of Guangdong Polytechnic Normal University (No. 10KJQ08).

References

1. R. Dorn, S. Quabis, and G. Leuchs, Phys. Rev. Lett. **91,** 233901 (2003).
2. Q. Zhan, Adv. Opt. Photon. **1,** 1 (2009).
3. X. Jia, Y. Wang, and B. Li, Opt. Express **18,** 7064 (2010).
4. D. Deng, J. Opt. Soc. Am. B **23,** 1228 (2006).
5. P. P. Banerjee, G. Cook, and D. R. Evans, J. Opt. Soc. Am. A **26,** 1366 (2009).
6. D. Deng and Q. Guo, Opt. Lett. **32,** 2711 (2007).
7. X. Jia, B. Li, and Y. Wang, Chin. Opt. Lett. **8,** 517 (2010).
8. C. Maurer, A. Jesacher, S. Furhapter, S. Bernet, and M. Ritsch-Marte, New J. Phys. **9,** 1 (2007).
9. A. Ito, Y. Kozawa, and S. Sato, J. Opt. Soc. Am. A **27,** 2072 (2010).
10. K. Huang, P. Shi, G. W. Cao, Ke Li, X. B. Zhang, and Y. P. Li, Opt. Lett. **36,** 888 (2011).
11. R. Martínez-Herrero, P. M. Mejías, S. Bosch, and A. Carnicer, J. Opt. Soc. Am. A **18,** 1678 (2001).
12. H. Guo, J. Chen, and S. Zhuang, Opt. Express **14,** 2095 (2006).
13. W. H. Carter, J. Opt. Soc. Am. **62,** 1195 (1972).
14. G. Zhou, Opt. Lett. **31,** 2616 (2006).
15. G. Wu, Q. Lou, and J. Zhou, Opt. Express **16,** 6417 (2008).
16. X. Kang and B. Lü, Opt. Commun. **262,** 1 (2006).